ARTICLE

True absolute determination of photoluminescence quantum yields by coupling multiwavelength thermal lens and photoluminescence spectroscopies

Received 00th January 20xx,
Accepted 00th January 20xx

DOI: 10.1039/x0xx00000x

Tatiane O. Pereira,[a] Monika Warzecha,[b] Luis H.C. Andrade,[a] Junior R. Silva,[a] Mauro L. Baesso,[c] Callum J. McHugh,[d] Jesus Calvo-Castro,[*e] and Sandro M. Lima[*a]

Photoluminescence quantum yields denote a critical variable to characterise a fluorophore and its potential performance. Their determination, by means of methodologies employing reference standard materials, innevitably leads to large uncertainties. In response to this, herein we report for the first time an innovative and elegant methodology, whereby the use of neat solvent/reference material required by thermal lens approaches is eliminated by coupling it to photoluminescence spectroscopy, allowing for the discrimination between materials with similar photoluminescence quantum yields. To achieve that, both radiative and non-radiative transitions are simultaneously measured by means of a photoluminescence spectrometer coupled to a multiwavelength thermal lens spectroscopy setup in a mode-mismatched dual-beam configuration, respectively. The absorption factor independent ratio of the thermal lens and photoluminescence signals can then be used to determine the fluorescence quantum yield both accurately and precisely. We validated our reported method by means of rhodamine 6G and further applied in three novel structurally related diketopyrrolopyrrole based materials to, contrary to results obtained by other methods, unveil significant differences in their photoluminescence quantum yields.

Introduction

Over the last decades, there has been an increasingly large surge of interest devoted to the development of novel fluorescent materials with superior performance to those currently existing ones and that can find applicability in a wide variety of topical fields, ranging from organic optoelectronics to bioimaging agents.[1–7] In addition to other photophysical parameters, such as the molar absorptivity and fluorescence lifetime, which are important in gauging the performance and/or suitability of a fluorophore for a specific application, the fluorescence quantum yield (Φ_f, Equation 1) is paramount in the characterization of a fluorophore.[8,9] It provides a measure of the efficiency of converting the absorbed photons into emitted ones and its product with the molar absorptivity (ε) gives the so-called fluorophore's brightness (B) at the excitation wavelength (λ_{exc}), $B = \Phi_f \cdot \varepsilon_{\lambda_{exc}}$. The photoluminescence quantum yield can be further expressed as the ratio between the rate of radiative decay (k_r) and the sum of the radiative and non-radiative (k_{nr}) decay process (Equation 1), where k_{nr} is used to group the rates of all possible non-radiative phenomena.[8,9]

$$\Phi_f = \frac{k_r}{k_r + k_{nr}} \qquad (1)$$

To date, the most widely used approach for the experimental determination of Φ_f is still the so-called optical relative method.[9–11] In this approach, the emission of the unknown sample is compared against that of a reference standard material for which the fluorescence quantum yield has been previously calculated, as illustrated by Equation 2.[9–11]

$$\frac{\Phi_{f,u}}{\Phi_{f,st}} = \frac{f_{st}}{f_u} \cdot \frac{F_u}{F} \cdot \frac{n_u^2}{n_{st}^2} \qquad (2)$$

Where the subscripts "u" and "st" denote the unknown sample and the fluorescence reference standard, respectively. In turn, f, F and n represent the absorption factor, the integrated emission spectrum and the refractive index, respectively. The absorption factor is a measurement of the fraction of the light irradiating the sample that is absorbed and can be denoted as $f = 1 - 10^{-A}$, where A is the absorbance. In cases where the solvent used for the unknown sample differs from that utilised for the reference standard material, a correction for n is employed. Despite its large popularity, likely as a consequence

[a] Programa de Pós-graduação em Recursos Naturais-PGRN, Centro de Estudos em Recursos Naturais-CERNA, Universidade Estadual de Mato Grosso do Sul-UEMS, 351, Dourados, MS, Brazil.
[b] EPSRC CMAC Future Manufacturing Research Hub, c/o Strathclyde Institute of Pharmacy and Biomedical Sciences, Technology and Innovation Centre, 99 George Street Glasgow, G1 1RD, U.K.
[c] Grupo de Estudos de Fenômenos Fototérmicos, Departamento de Física, Universidade Estadual de Maringá, Av. Colombo 5790, 87020-900 Maringá, PR, Brazil.
[d] School of Computing, Engineering and Physical Sciences, University of the West of Scotland, Paisley, PA1 2BE, U.K.
[e] School of Life and Medical Sciences, University of Hertfordshire, Hatfield, AL10 9AB, U.K.

Electronic Supplementary Information (ESI) available: Full details for the synthesis of **TPADPP**, **mTPADPP** and **mDMADPP**. See DOI: 10.1039/x0xx00000x

of required instrumentation being readily available in most research laboratories, the method suffers from a number of shortcomings which often inevitably lead to large uncertainties of ca 10%.[9–12] To a large extent these can be attributed to i) the recommendation of utilising identical excitation wavelengths for both reference standard and unknown material, often resulting in values located on the edge of the main absorption band of the unknown sample, ii) the appropriate correction of the emission spectra to account for non-linear responses of detectors and more importantly iii) the availability of suitable photoluminescence reference standard materials and the accuracy to which their quantum yields have been previously determined.[8–14]

In an attempt to bypass the latter, the so-called absolute methods have been developed, whereby Φ_f values are determined by directly measuring the number of photons absorbed and emitted and which has been facilitated by the commercial availability of integrating spheres.[9,12,15–17] However, the reliability of the obtained photoluminescence values with this method is subjected to the manufacturer correction methodologies as well as to the careful account of self-absorption effect, particularly in those materials where there is a large overlap between the absorption and fluorescence emission spectra.[18] Alternatively, the thermal phenomena occurring as a result of material irradiation can also be exploited for the experimental indirect determination of Φ_f by photothermal methods, such as photoacoustic spectroscopy,[19–21] photothermal deflection spectroscopy,[22] thermal lens spectroscopy (TLS)[23–26] and other calorimetric approaches[27] which are often believed to be less sensitive to errors than optical-based approaches. Whilst both photoacoustic and thermal lens spectroscopies are photothermal methods, their underlying physical principle is different from one another. In short, photoacoustic methods, which are based on determining the acoustic waves generated following sample irradiation, have been extensively employed as alternative approaches to optical-based methods for the photoluminescence quantum yield determination. However, they suffer from pitfalls such as the lack of reproducibility and sensitivity range between the acoustic transducer and the sample. In turn, the basic principle of TLS is the generation of a local heat-induced thermal gradient which creates a refractive index profile upon sample irradiation and that results in the generation of a lens-like effect. Importantly, although both methods are often referred to in the literature as absolute methods, they both require the use of a material exhibiting complete heat conversion, so-called reference material. This role is often played by the neat solvent employed in solution-phase measurements, which can however lead to uncertainties in the experimental determination of Φ_f. In short, among other experimental variables, these uncertainties can be further ascribed to the erroneous assumption that both reference material and sample exhibit negligible changes in viscosity. In fact, a significant increase in viscosity is often observed upon addition of the fluorophore when compared to the neat solvent, which results in changes to the thermal diffusivity of the sample with respect to the 'reference sample' and leads to errors in determined photoluminescence quantum yields. The latter is of particular concern when there are small differences between Φ_f for a set of fluorophores, such as studies whereby the aim is to investigate the effect that small systematic substitutions performed on common core motifs have on their photophysical properties, a commonly employed approach in the rational development of novel materials.

Motivated by these shortcomings, herein we report on the application of a novel and elegant approach for the absolute determination of photoluminescence quantum yields in solution phase by simultaneously coupling multiwavelength thermal lens and photoluminescence spectroscopies. To the best of our knowledge this is the first report of a method whereby the experimental determination of Φ_f is achieved without the need for normalising the thermal lens (TL) signal with the literature reported for the solvent or determining the absorption coefficient, hence alleviating the aforementioned concerns. To achieve that, simultaneous measurements of both the radiative and non-radiative transitions generated by the sample upon excitation were collected by an optical fiber connected to the spectrometer and a multiwavelength TLS setup in a mode-mismatched dual-beam, respectively. By simultaneously irradiating the sample with the same excitation power for thermal lens (θ) and photoluminescence (I_f) spectroscopy measurements, their absorption factors can be cancelled out. The resultant, excitation energy independent parameter (θ/I_f), exhibits a linear relationship with the excitation wavelength, hence allowing for the absolute determination of Φ_f.

Similarly to most studies in the field,[11,20,24–26] we first validated our experimental setup by means of the widely-employed primary photoluminescence reference standard material rhodamine 6G, for which results comparable to those in the literature were obtained. Whilst other, so-called secondary reference standards, are routinely used for the validation of experimental methods,[13,20,22,28] our choice of a primary reference standard material such as rhodamine 6G is underpinned by i) this dye being, alongside quinine sulphate and fluorescein, one of the only three recommended standard materials by IUPAC guidelines[28] and ii) rhodamine 6G exhibiting the larger spectral similarities to the three novel materials reported herein when compared to the other primary reference standards. Subsequently, we used this methodology to further test it by determining the Φ_f of three novel and structurally related diketopyrrolopyrrole (DPP) based materials, where the systematic substitutions are anticipated to lead to small changes in the photoluminescence efficiency. Along these lines, we are engaged in the rational development of organic optoelectronic materials exploiting DPP chemistries exhibiting superior properties to those currently existing ones and that can find applicabilities as chemical sensors by selectively modulating their intrinsic fluorescence properties.[7,29] In short, DPPs have been widely used for decades as high performance pigments due to their excellent properties[30–34] and more recently have seen an increasingly large surge of interest as charge transfer mediating materials in optoelectronic applications.[31,35,36] Herein, we synthesise, purify and

characterise the photophysical properties of three novel architectures, with special focus to the experimental determination of the photoluminescence quantum yields. In light of the results reported in this work, with Φ_f > 0.81 in all cases and their functionalities, we anticipate them to be of interest as fluorescent sensors for nitroaromatic compounds which we will be reporting elsewhere. The three architectures received names in the form of XDPP, where X denotes their substitution on the para position of the core phenyl ring(s) and the prefix 'm' indicates that only one of the core rings is substituted and the system is therefore non-symmetrical (Figure 1). In line with their different substitutions on the para positions of the core rings, their quantum yields were observed to exhibit small but relevant differences (e.g. Φ_f = 0.89 ± 0.03, 0.81 ± 0.02 and 0.94 ± 0.03 for **TPADPP**, **mTPADPP** and **mDMADPP** in dichloromethane, respectively) and therefore represent an appropriate dataset to further challenge our methodology. The ability to discriminate between fluorophores with similar Φ_f is deemed important in the understanding of the impact of structural modifications bear on the photophysical properties excited state radiative and non-radiative deactivation pathways. As a result, we anticipate this work to be of interest to the large scientific community engaged in the development of novel methodologies for the experimental determination of photoluminescence quantum yields as well as those devoted to the realisation of new architectures for which accurate values of Φ_f are critical.

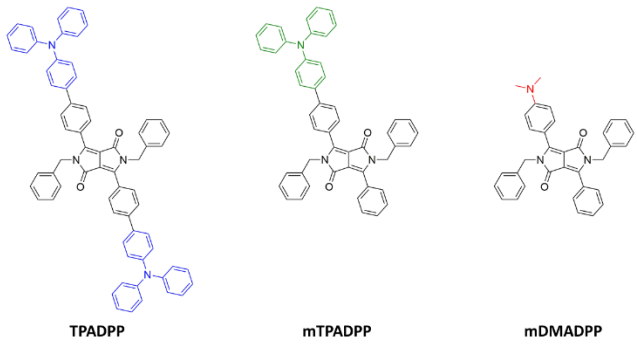

Figure 1. Chemical structures for **TPADPP**, **mTPADPP** and **mDMADPP** (see SI1 for details).

Materials and Methods

Chemical and Reagents. HPLC grade dichloromethane was purchased from Fisher-Scientific and used without any further purification. Diketopyrrolopyrrole-based materials were all synthesized, purified and characterized following our previously described methodology. Rhodamine 6G photoluminescence reference standard was purchased from Sigma-Aldrich and used as supplied.

Instrumentation. All experimental spectroscopic measurements were carried out in a temperature-controlled laboratory at 24 °C unless otherwise stated. In all cases, diluted solutions were experimentally evaluated, exhibiting concentrations in the range of μM and always characterised by optical densities below 0.1 at the excitation wavelength. Steady-state absorption spectrophotometry measurements were carried out employing a Perkin-Elmer Lambda 1050 UV/Vis spectrophotometer, operated by the software UV WinLab v.2.80.03 supplied by the manufacturer. Absorption spectra were recorded in the region of 350 to 600 nm. The photoluminescence (PL) and photoluminescence excitation (PLE) spectra of the materials investigated were obtained by means of a Perkin-Elmer LS55 luminescence spectrometer, operated with the software UV WinLab v.4.00.03 supplied by the manufacturer. Samples were irradiated utilising a Xe lamp and simultaneous excitation-emission spectra contour plots (maps) were obtained by selecting excitation wavelengths in the region of 250-600 nm (5 nm steps) and the PL spectra recorded from 500 to 800 nm, with a 1 nm resolution (simultaneous excitation-emission maps in Figure 4 illustrate emission wavelengths up to 750 nm due to the small intensities at longer wavelengths as illustrated in Figure 3). The PL was recorded by a Hamamatsu R928 photomultiplier tube coupled to the luminescence spectrometer. The obtained PL spectra were corrected for the intensity of the Xe lamp and the response of the photomultiplier tube with a file supplied by the manufacturer which accounts for its non-linear response in the spectral region of interest. All measurements were carried out in standard 10 mm precision quartz cuvettes purchased from Hellma-Analytics, at room temperature and under aerated conditions unless otherwise stated.

Thermal lens spectroscopy. Diluted solutions(Optical density < 0.1) of the diketopyrrolopyrrole-based materials in dichloromethane and Rhodamine 6G in ethanol were analysed by time-resolved TLS utilising a dual-beam mode-mismatched configuration as illustrated in Figure 2.

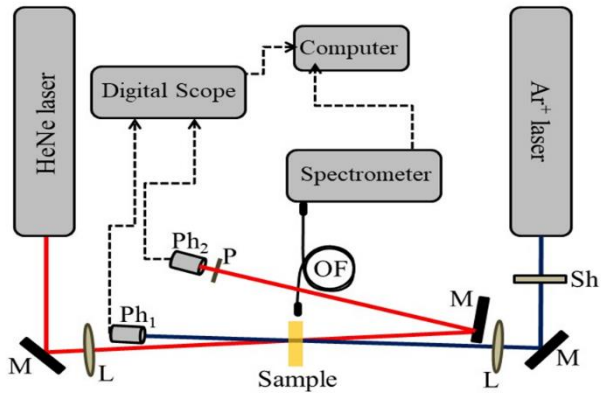

Figure 2. Block diagram illustration of the dual-beam mode-mismatched thermal lens spectroscopy experimental setup utilised in this work, where Sh, M and L denote the shutter, flat mirrors and biconvex lenses respectively. In turn, P, Ph and OF represent the pinhole, photodetectors and optical fibre respectively.

In the illustrated experimental setup in Figure 2, the first photodetector (Ph_1) is used to trigger the digital scope (TBS 2000, purchased from Tektronix) and the shutter (Sh) controls the exposure of the sample to the excitation laser. The sample is then presented contained in a quartz cuvette with a (1.00 ±

0.05) mm path length and located at the position of minimum waist of the excitation beam, an Innova 308C Ar^+ laser from Coherent. This laser was tuned to excite the samples at wavelengths, λ_{exc} = 457.9, 476.5, 496.5 and 514.5 nm. In turn, the thermal lens effect was probed by a 632.8 nm HeNe laser, also from Coherent, which passes through the sample almost collinear through the excitation beam. Both beams are Gaussian and have transverse electromagnetic fundamental mode (TEM_{00}), which denotes a condition for the application of the theoretical TLS model. In this regard, the reader should note that our proposed methodology is not solely limited to the lasers described herein and that in fact, other commercially available ones with the above-mentioned characteristics can be used. Our choice of the probe laser was underpinned by its low power and a wavelength outside the main absorption band of the materials investigated.

In short, the basic principle of the TLS is the use of the excitation laser beam to create a local thermal gradient, generating a refractive index profile which in turn induces the sample to behave as a lens-like element as a consequence of the absorbed energy being converted into heat by the sample. Subsequently, crossing of the sample heated region with the probe laser, i.e. 632.8 nm HeNe laser in our work, results in the far-field observation of the divergence of the beam. Monitoring the time-dependence of this TL effect (amplitude of the signal) with the second photodetector (Ph_2, Figure 2) allows for the experimental determination of critical thermo-optical parameters such as the thermal diffusivity (*D*), the temperature dependence of the refractive index (*dn/dT*) as well as the fraction of absorbed energy which is converted into heat by the sample (φ). Both photodetectors, Ph_1 and Ph_2 in Figure 2 are germanium-based with rise times < 100 ps, bandwidth > 3.0 GHz and spectral range from 400 to 2000 nm. Optical fibres employed in our experimental setup were purchased from Ocean Optics, with a diameter of 300 µm, length of 1 m and wavelength range 300-1100 nm.

Subsequently, the data was fitted employing a previously reported theoretical model, where the so-called on-axis transient intensity of the probe beam, $I(t)$, in the far field can be expressed using the following Equation 3:[37,38]

$$I(t) = I(0)[1 - \frac{\theta}{2}\arctan(\beta)]^2 \qquad (3)$$

$$\beta = \frac{2mV}{[(1+2m)^2 + V^2]\left(\frac{t_c}{2t}\right) + 1 + 2m + V^2}$$

where $I(0)$ denotes the signal intensity for $t = 0$ or $\theta = 0$. t_c, which represents the TL characteristic time constant can be expressed as $t_c = w_{oe}^2/4D$, where w_{oe} and *D* denote the radius of the excitation beam waist at the sample position and the thermal diffusivity of the sample, respectively. In turn, *m* and *V* are both intrinsic geometrical parameters related to the probe and excitation lasers, respectively. The parameter *m* can be further denoted as the square ratio between the radius of the probe beam at the sample position (w_{lp}) and w_{oe}. *V* represents the ratio between Z_1 and Z_{cp}, which represent the distance between the minimum beam waist and the sample position at the probe axis and the confocal parameter of the probe beam, respectively. Z_{cp} can be further equated to $\pi w_{op}^2/\lambda_p$, where w_{op} denotes the minimum beam radius of the probe laser wavelength (λ_p). Herein, we utilised w_{oe} = (125 ± 1) µm, w_{op} = (127 ± 3) µm, Z_1 = (0.238 ± 0.005) m and Z_{cp} = (0.074 ± 0.005) m. Within the framework of Shen's model,[38] the amplitude of the TL signal is proportional to θ, the thermally induced phase difference of the probe beam for a radius, *r* = 0 and *r* ~$1.41w_{oe}$ ($\vartheta < 0.1$), given by:[37–39]

$$\theta = -\frac{P_{in}\alpha L_{eff}}{\lambda_p K}\varphi\left(\frac{dn}{dT}\right) \qquad (4)$$

Where P_{in} and α represent the excitation power and the absorption coefficient at the excitation wavelength (λ_{exc}), respectively. $L_{eff} = (1 - e^{-\alpha L})/\alpha$ is the sample effective thickness. The thermal conductivity, $K = \rho CD$, where ρ denotes the volumetric density and *C* the specific heat capacity of the sample. φ, which is the fraction of the absorbed energy converted into heat by the sample, is related to Φ_f as follows:[39]

$$\varphi = 1 - \Phi_f\left(\frac{\lambda_{exc}}{\lambda_{em}}\right) \qquad (5)$$

where λ_{em} is the average emission wavelength. In this work, the TLS approach was employed to determine Φ_f by fixing the excitation wavelength as well as simultaneously measuring both the radiative and nonradiative transitions of the sample upon excitation. Whilst the radiative emission signal is collected by an optical fiber connected to the spectrometer (Figure 2), the non-radiative transitions are monitored by TLS operated in the mode-mismatched dual-beam configuration for multiwavelength excitations.

Results and Discussion

Steady-state absorption and fluorescence emission. Firstly, the steady-state absorption and fluorescence emission spectral properties were investigated for the three amine-substituted diketopyrrolopyrrole materials in the solvent of dichloromethane to, i) aid in the selection of the experimental parameters to be utilised in the determination of Φ_f and ii) characterise these novel materials that could pave the way for their subsequent potential application. All three DPP-based materials exhibit broad and strong (ε = 4.6, 2.7 and 2.7 x 10^5 M^{-1} cm^{-1} for **TPADPP**, **mTPADPP** and **mDMADPP** in dichloromethane, respectively) absorption bands in the visible region, with no observable vibronic progression, consistent with DPP systems bearing phenyl core rings.[29,31]

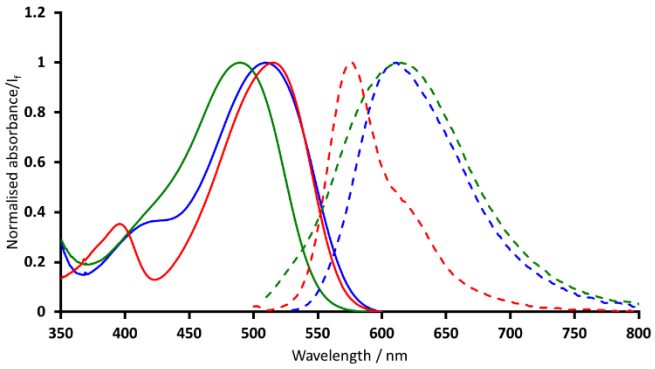

Figure 3. Normalised absorption (solid line) and fluorescence emission (dashed line) spectra of **TPADPP** (blue), **mTPADPP** (green) and **mDMADPP** (red) in dichloromethane.

These bands, which can be attributed to π-π* transitions in all cases,[31] are centred at ca 509, 490 and 516 nm for **TPADPP**, **mTPADPP** and **mDMADPP** respectively, thus indicating significant absorption of all three materials at the Ar^+ laser lines which will be utilised as the excitation source in the multiwavelength TLS work. It is apparent the bathochromic shift on progression from **mTPADPP** to its symmetrical analogue **TPADPP**, consistent with an increase in the conjugation along the so-called long molecular axis of DPPs.[40] Of note is the observed absorption maximum for **mDMADPP**, the largest of all three investigated systems. In this regard, we attribute the ca 26 nm bathochromic shift on progression from **mTPADPP** to **mDMADPP** to a more efficient contribution of the lone pair of electrons in the amine nitrogen towards enhancing the conjugation in the latter due to additional phenyl ring and associated greater twist of the core ring in the case of **mTPADPP** (Figure 1).

Fluorescence emission spectra of **TPADPP** and **mTPADPP** are both broad and unresolved (FWHM ca 3000 and 2800 cm^{-1} for **TPADPP** and **mTPADPP** respectively), exhibiting negligible differences in their emission maxima (λ_{em}^{max} = 612 and 613 nm for **TPADPP** and **mTPADPP**, respectively). The fluorescence emission spectra of **mDMADPP** exhibits the narrowest spectral envelope, with a FWHM of ca 1500 cm^{-1}. Contrary to the observations made for the absorption spectra of the three materials, a clear hypsochromic shift was observed in the photoluminescence spectra when comparing **mDMADPP** (λ_{em}^{max} = 576 nm) with its aromatic amine bearing counterparts. Along these lines, it is known that DPP-based materials undergo a planarization of the core rings with respect to the core on progression from ground state to excited state relaxed geometries.[31,41] Thus, we attribute these findings to smaller changes in core rings torsion in **mDMADPP** due to its more planar ground state geometry when compared to the other two materials (vide supra). The latter explanation is further supported by the observed significant differences in observed Stokes shifts ($\Delta\lambda_{max}$ = 3306, 4095 and 2019 cm^{-1} for **TPADPP**, **mTPADPP** and **mDMADPP**, respectively). The average emission wavelength, λ_{em} were determined by integrating the fluorescence emission spectra (Table 1), with yielded values consistent with the aforementioned emission maxima and FWHM. Further, we report in all cases fluorescence emission spectral shapes which are irrespective of the excitation wavelength, as illustrated in Figure 4. In this regard, it is of particular note the lack of changes in the emission maxima at the different excitation wavelengths that will be employed in the multiwavelength thermal lens studies (λ_{exc} = 457.9, 476.5, 496.5 and 514.5 nm).

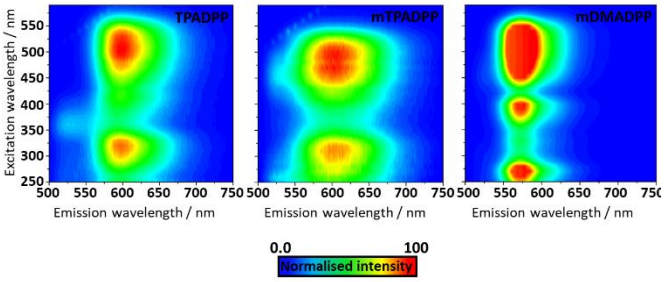

Figure 4. Excitation-emission maps for **TPADPP** (left), **mTPADPP** (centre) and **mDMADPP** (right) in the solvent of dichloromethane.

Comparison of the steady-state absorption and fluorescence emission spectra of the DPP-based architectures in dichloromethane with these of our benchmarking material, rhodamine 6G in ethanol is consistent with broader spectra for the DPP materials in all cases and larger spectral overlap in the case of rhodamine 6G. In this regard, we anticipate lower probability of self-absorption processes in these novel materials which broadens their applicabilities as photonic materials.[31,42]

Photoluminescence quantum yield determination by thermal lens spectroscopy with reference sample. The photoluminescence quantum yields for the DPP materials were first determined by means of TLS employing the so-called method with reference sample.[39] The TL transient signals for all three novel materials were measured with excitation wavelengths at 476.5 nm in all cases and excitation powers ranging from 0.13 to 1.29 mW, to evaluate linear dependence of the thermal lens signal amplitude, θ with 5-8 different excitation powers. Maximum excitation powers were carefully selected as to avoid θ values greater than 0.2, which can compromise reproducibility of the results[39]

In all cases, we observed divergent TL transients, which are consistent with measurements in solution phase. Transients were then fitted employing Equation 3 and the obtained amplitudes plotted against the excitation power to evaluate the linear dependence (Figure 5D) as well as to further determine the θ/P_{in} utilising Equation 4 (Table 1).The absorption coefficient at λ_{exc} = 476.5 nm were calculated from the absorption coefficient spectra and are summarised in Table 1 as their product with the effective thickness, L_{eff}. Subsequently, these were then used to determine the TL signal normalised by the absorbed power (P_{in}/L_{eff}) to obtain $\Theta_{sample} = \theta/P_{in}\alpha L_{eff}$. The fraction of absorbed energy converted into heat for each sample was obtained by dividing Θ_{sample} by that of the solvent (reference sample, $\Theta_{solvent} = (1/\lambda_p K)dn/dT$) determined by using literature data for K = 0.122 $Wm^{-1}K^{-1}$ and $dn/dT = 5.5 \times 10^{-4}$ K^{-1}.[43] Lastly, the photoluminescence quantum yields were

determined and are summarised in Table 1 along with the parameters utilised to calculate them using Equation 4 and 5.
In all cases we report high photoluminescence quantum yields, consistent with previously reported values for other DPP-based architectures.[31] Of particular note is the Φ_f close to unity determined for **mDMADPP** under de-aerated conditions, which highlights the lack of significant non-radiative deactivation mechanisms for this derivative and places it among the highest reported values for N-benzyl substituted DPPs.[29,31] In addition, to further understand the TL processes in these novel systems, we went on to determine the characteristic time constant for the TL phenomenon in these materials, t_c. The latter allowed us to calculate the thermal diffusivity of the samples, D, employing $t_c = w_{oe}^2/4D$ for w_{oe} = 125 µm (Table 1). Both triphenylamine-bearing derivatives, **TPADPP** and **mTPADPP** exhibit similar values which are ca 10% larger than the one obtained for their counterpart **mDMADPP** (D = 1.08, 1.06 and 0.96 $\times 10^{-3}$ cm^2 s^{-1} for **TPADPP**, **mTPADPP** and **mDMADPP** in dichloromethane, respectively), which we attribute to the different molecular size and solution viscosity.[44] Along those lines, we determined a thermal diffusivity for neat dichloromethane solution of 0.84 $\times$ 10^{-3} cm^2 s^{-1}, which is ca 8% larger than the often utilised literature value,[43] consistent with acceptable solvent purity changes among suppliers. Importantly, the experimental determination of Φ_f in solution by TLS, assumes negligible differences between D of sample and solvent (reference).

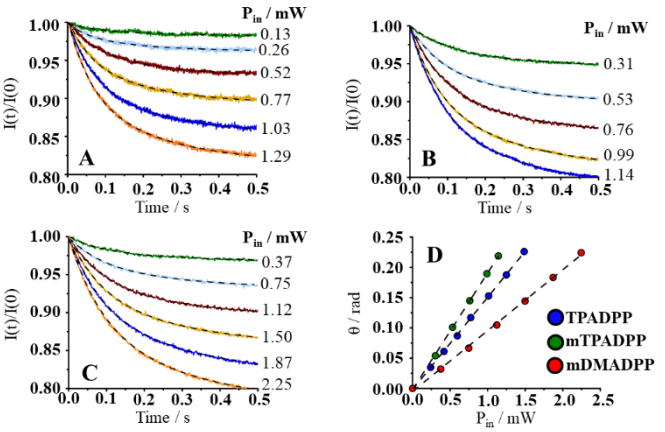

Figure 5. Average (n=10) time-resolved thermal lens transient signals for **TPADPP** (**A**), **mTPADPP** (**B**) and **mDMADPP** (**C**) in dichloromethane (λ_{exc} = 476.5nm). Illustrated theoretical fits were calculated using Equation 3. **D** Thermal lens amplitude signals at 476.5 nm calculated from the theoretical fits as a function of the excitation power for **TPADPP** (blue filled circles), **mTPADPP** (green filled circles) and **mDMADPP** (red filled circles) in dichloromethane. Dashed lines illustrate linear regressions.

Table 1. Average emission wavelengths (λ_{em}), thermal diffusivity for w_{oe} = 125 µm (D), thermal lens signals (θ) obtained for λ_{exc} = 476.5 nm and normalised for the incident excitation power (P_{in}), product of the absorption coefficient (α) and the effective thickness (L_{eff}) for λ_{exc} = 476.5 nm, thermal lens signal normalised for the absorbed power (Θ), fraction of the absorbed energy converted into heat (φ) and photoluminescence quantum yield (Φ_f)

System	λ_{em} / nm	D / 10^{-3} cm^2/s ±2.5%	θ/P_{in} / W^{-1} ±2.5%	αL_{eff} ±1.5%	Θ_{sample} / W^{-1} ±3.0%	φ ±3.0%	Φ_f ±3.0%
TPADPP	603	1.08	151	0.071	2124	0.300	0.85
mTPADPP	599	1.06	189	0.082	2287	0.320	0.82
mDMADPP	573	0.96	103	0.076	1360	0.190	0.94

In cases where differences are observed, these are often associated to changes in the thermal properties of the system, namely the temperature dependence of the refractive index, dn/dT, and the thermal conductivity, K, resulting in errors in the experimentally determined values. Motivated by these shortcomings, we went on to develop a novel approach for the determination of Φ_f whereby multiwavelength TLS is combined with photoluminescence spectroscopy for the true absolute determination of the photoluminescence quantum yields without the need for $\Theta_{solvent}$ literature data.

Photoluminescence quantum yield determination by simultaneous multiwavelength thermal lens and photoluminescence spectroscopy. We demonstrate the experimental determination of the photoluminescence quantum yields by simultaneously measuring both the radiative and nonradiative mechanisms upon sample excitation. By simultaneously measuring the thermal lens and photoluminescence signals following excitation with identical power (θ/Pin and If/Pin, respectively), the term accounting for the number of absorbed photons can be cancelled out and the parameter θ/If can be calculated. Importantly, this parameter exhibits a linear dependence with the excitation energy where the gradient is furthermore proportional to the photoluminescence quantum yield.

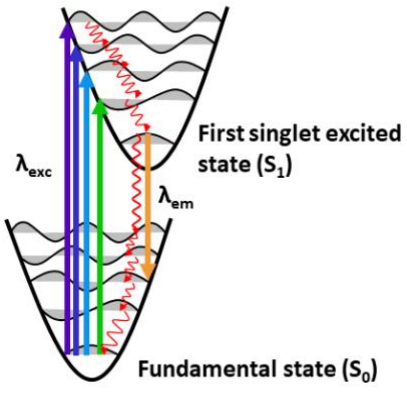

Figure 6. Illustration of the radiative (orange straight arrow) and nonradiative (red wavy arrows) transitions following sample excitation at different wavelengths (λ_{exc} = 514.5, 496.5, 476.5 and 457.9 nm) in a two energy-level diagram.

Using this novel approach, we first validated it by means of the widely employed reference standard material rhodamine 6G to then determined the Φ_f for the three investigated DPP-based materials and compared their values to those obtained by the previously described method using a reference sample. Whilst the radiative signal is collected by an optical fibre connected to the spectrometer (Figure 2), the non-radiative transitions are measured by means of TLS in mode-mismatched dual-beam setup employing different excitation wavelengths. Figure 6 illustrates the radiative and non-radiative deactivation mechanisms following multiwavelength sample excitation utilising a simple two-level energy diagram. It is of note that the proposed method requires negligible changes in the spectral shape of the photoluminescence spectrum to occur at the different excitation wavelengths employed (*vide supra*). In all cases we observed that in agreement with Equation 5, the amplitude of the TL signal increases as the excitation wavelength decreases. The latter can be ascribed to an increase in the amount of absorbed energy that is converted into heat as the excitation wavelength decreases (Figure 6).

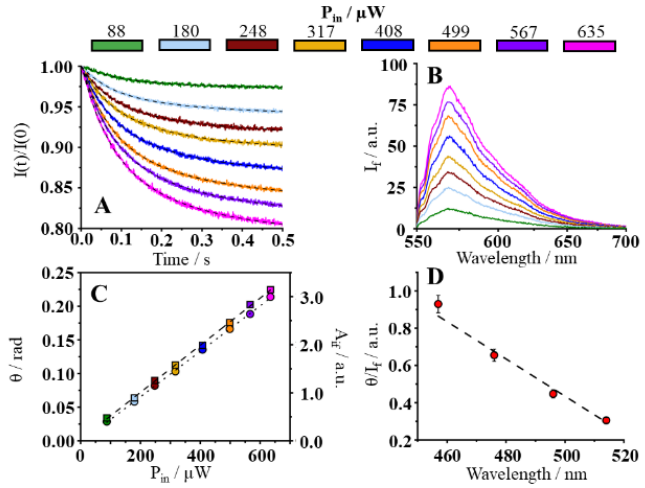

Figure 7. **A** Characteristic average (n=10) time-resolved TL transients for rhodamine 6G in ethanol for λ_{exc} = 476.5 nm at different excitation powers. Black dashed lines denote theoretical fits utilising Equation 3. **B** Steady-state fluorescence emission spectra of rhodamine 6G in ethanol for λ_{exc} = 476.5 nm at different excitation powers. **C** Amplitude of the thermal lens signal (ϑ, filled circles) and area under the fluorescence emission spectra (filled squares) as a function of the excitation power. **D** Normalised thermal lens signal as a function of the excitation wavelength (dashed line illustrates linear fit).

Figure 7 illustrates the time-resolved thermal lens transients (7A) and steady-state photoluminescence spectra (7B) of rhodamine 6G in ethanol at different excitation powers at λ_{exc} = 476.5 nm. Similar behaviour was also observed for excitation wavelengths at 457.9, 496.5 and 514.5 nm. We report that, in all cases the amplitude of the signals exhibits a linear relationship with the excitation power, hence consistent with equal number of photons in prior to measured radiative and nonradiative processes (Figure 7C) which allows for the determination of the TL and photoluminescence signals normalised for the excitation power. The photoluminescence quantum yield is then calculated since the parameter θ/I_f is proportional to the fraction of absorbed energy converted into heat (φ) by means of Equation 5. We report Φ_f of ca 1.00 - 0.00/+0.05 for rhodamine 6G in ethanol (for λ_{em} = 551 nm) by our novel approach, which is in good agreement with previously reported studies reporting experimentally determined photoluminescence quantum yields for this primary reference standard of 1.00 +0.00/-0.05, 0.97 +0.03/-0.07 and 0.95 ±0.05.[20,28,45]

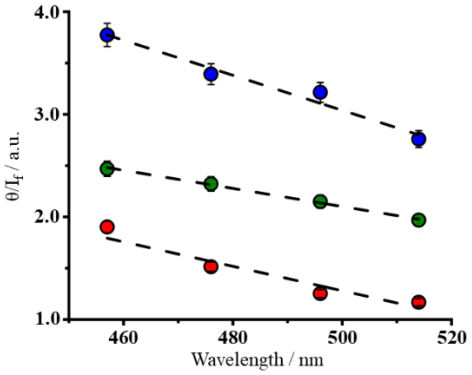

Figure 8. θ/I_f as a function of the excitation wavelength for **TPADPP** (blue filled circles), **mTPADPP** (green filled circles) and **mDMADPP** (red filled circles) in dichloromethane. Solid lines denote linear fits with correlation coefficients, r^2 of 0.9897, 0.9984 and 0.9811 for **TPADPP**, **mTPADPP** and **mDMADPP** respectively.

We devote the remaining of the manuscript to the determination of the photoluminescence quantum yields of the three investigated diketopyrrolopyrrole architectures in dichloromethane utilising our newly developed methodology. Figure 8 illustrates the ratio of the normalised thermal lens and photoluminescence signal for the excitation power as a function of the excitation wavelength. We observed linear relationships in all cases, where the fraction of absorbed photons converted into heat is inversely proportional to the excitation wavelength (Figure 6) and no predicted convergence as λ_{exc} tends to zero. The latter is consistent with the previous observation that the thermo-optical properties of DPP-containing solutions vary with respect to those determined for neat dichloromethane, which led to errors in Φ_f and warrants the development of novel experimental methodologies. Similarly to the case detailed for rhodamine 6G, the photoluminescence quantum yields can be obtained for the gradients of the linear fits in Figure 8 employing Equation 5. For all three investigated materials we report (Φ_f = 0.89 ± 0.03, 0.81 ± 0.02 and 0.94 ± 0.03 for **TPADPP**, **mTPADPP** and **mDMADPP**, respectively) interesting observations when these values are compared to those yielded by the method employing a reference sample, particularly in the case of**TPADPP** (Φ_f = 0.81 ± 0.02 by means of the method with the reference sample), which now exhibits small but significant differences with respect to its asymmetrical counterpart **mTPADPP**. This increase in photoluminescence quantum yield on progression from triphenylamino- to dimethylamino-bearing systems can be accounted for by means of the observed hypsochromic shift in the emission spectra of **mDMADPP** (λ_{em} = 576 nm) when compared to **TPADPP** (λ_{em} = 612 nm) and **mTPADPP** (λ_{em} = 613 nm). The latter can be associated to a lower lying LUMO level and narrower energy gap. Thus, within

the formalism of the Fermi Golden Rule of perturbation theory and the Equations derived from the Energy Gap Law,[46–49] these experimental observations are consistent with materials with larger energy gaps being characterised by larger radiationless decay rate constants and hence lower photoluminescence efficiencies (Equation 1). The experimentally determined photoluminescence quantum yields for these novel materials highlight the importance of accurate and precise determination of photoluminescence quantum yields, particularly in cases where small systematic substitutions performed to core motifs result in small variation in the photophysical properties and further warrants the development of superior experimental methodologies like the one reported in this work.

Conclusions

In conclusion, a novel method for the experimental determination of photoluminescence quantum yields in diluted solutions is reported and ratified whereby the need for a reference sample is eliminated. Herein, we demonstrate that by simultaneously measuring both the radiative and nonradiative transitions upon sample irradiation, the photoluminescence efficiency can be determined. To do that, we collected the radiative signal by an optical fibre connected to a spectrometer and the non-radiative transitions by means of thermal lens spectroscopy in mode-mismatched dual-beam configuration employing different excitation wavelengths. As such, the resulting absorption power independent parameter denoting the ratio of both thermal lens and photoluminescence signals can be utilised to determine the quantum yields in a true absolute manner since it exhibits a linear dependence with the excitation wavelength. In line with most studies in the field, we tested and validated our developed method for liquid samples by means of rhodamine 6G. In light of our interest in the development of novel organic optoelectronic materials and the understanding that small systematic substitutions bear on their photophysical properties, we went on and synthesized three novel diketopyrrolopyrrole-based architectures. Their photophysical properties where evaluated in detail with special focus given to the photoluminescence quantum yields. Interestingly, we observed that by employing the novel approach we were able to discriminate between the quantum yields of two systems which we were previously unable to do utilising another methodology. Our proposed approach not only denotes an elegant way of determining the photoluminescence efficiency without the need for a reference material but has further demonstrated an ability to aid in the investigation of the effect that systematic substitutions bear on the photophysical properties, particularly in cases where these are small but relevant. As a result, we believe this work should be of interest to those developing novel methodologies for the accurate and precise determination and to those engaged in the rational realisation of organic optoelectronic materials with superior properties.

Conflicts of interest

There are no conflicts to declare.

Acknowledgements

The authors acknowledge funding from the Coordenação de Aperfeiçoamento de Pessoal a Nível Superior (CAPES, 88881.132572/2016-01 (T.O.P.)), Conselho Nacional de Desenvolvimento Científico e Tecnológico (CNPq, grants 305067/2019-2 (S.M.L.), 306452/2018-9 (LHCA), 425930/2018-1, 422329/2018-5 (J.C.C. and S.M.L.) and 310772/2019-2 (J.R.S.)) and Financiadora de Estudos e Projetos (FINEP, 01.08.0565.01). C.J.M and M.W. acknowledge EPSRC for funding under the First Grant Scheme [EP/J011746/1].

Notes and references

1 T. L. Mako, J. M. Racicot and M. Levine, *Chem. Rev.*, 2019, **119**, 322–477.
2 A. Hagfeldt, G. Boschloo, L. Sun, L. Kloo and H. Pettersson, *Chem. Rev.*, 2010, **110**, 6595–6663.
3 H. M. Kim and B. R. Cho, *Chem. Rev.*, 2015, **115**, 5014–5055.
4 O. Ostroverkhova, *Chem. Rev.*, 2016, **116**, 13279–13412.
5 Y. Yang, Q. Zhao, W. Feng and F. Li, *Chem. Rev.*, 2013, **113**, 192–270.
6 L. You, D. Zha and E. V. Anslyn, *Chem. Rev.*, 2015, **115**, 7840–7892.
7 T. F. Abelha, G. Morris, S. M. Lima, L. H. C. Andrade, A. J. McLean, C. Alexander, J. Calvo-Castro and C. J. McHugh, *Chem. – Eur. J.*, 2020, **26**, 3173–3180.
8 J. R. Lakowicz, *Principles of Fluorescence Spectroscopy*, Springer, 3rd edn., 2006.
9 C. Würth, M. Grabolle, J. Pauli, M. Spieles and U. Resch-Genger, *Nat. Protoc.*, 2013, **8**, 1535–1550.
10 C. A. Parker and W. T. Rees, *Analyst*, 1960, **85**, 14.
11 J. N. Demas and G. A. Crosby, *J. Phys. Chem.*, 1971, **75**, 991-.
12 K. Rurack, ed. U. Resch-Genger, Springer Berlin Heidelberg, 2008, vol. 5, pp. 101–145.
13 U. Resch-Genger, D. Pfeifer, C. Monte, W. Pilz, A. Hoffmann, M. Spieles, K. Rurack, J. Hollandt, D. Taubert, B. Schonenberger and P. Nording, *J. Fluoresc.*, 2005, **15**, 315–336.
14 K. Rurack and M. Spieles, *Anal. Chem.*, 2011, **83**, 1232–1242.
15 J. C. De Mello, H. F. Wittmann and R. H. Friend, *Adv. Mater.*, 1997, **9**, 230–232.
16 K. Suzuki, A. Kobayashi, S. Kaneko, K. Takehira, T. Yoshihara, H. Ishida, Y. Shiina, S. Oishic and S. Tobita, *Phys. Chem. Chem. Phys.*, 2009, **11**, 9850–9860.
17 L. Porrès, A. Holland, L.-O. Pålsson, A. P. Monkman, C. Kemp and A. Beeby, *J. Fluoresc.*, 2006, **16**, 267–272.
18 S. Leyre, E. Coutino-Gonzalez, J. J. Joos, J. Ryckaert, Y. Meuret, D. Poelman, P. F. Smet, G. Durinck, J. Hofkens, G. Deconinck and P. Hanselaer, *Rev. Sci. Instrum.*, , DOI:10.1063/1.4903852.
19 M. G. Rockley and K. M. Waugh, *Chem. Phys. Lett.*, 1978, **54**, 597–599.
20 C. Würth, M. G. González, R. Niessner, U. Panne, C. Haisch and U. R. Genger, *Talanta*, 2012, **90**, 30–37.
21 T. Schmid, U. Panne, R. Niessner and C. Haisch, *Anal. Chem.*, 2009, **81**, 2403–2409.
22 B. Couch, A. Meyer, B. Heller and S. L. Johnson, *Methods Appl. Fluoresc.*, 2018, **7**, 015004.

23 S. M. Lima, A. K. R. Souza, A. P. Langaro, J. R. Silva, F. B. Costa, J. C. S. Moraes, M. S. Figueiredo, F. A. Santos, M. L. Baesso, L. A. O. Nunes and L. H. C. Andrade, *Opt. Mater.*, 2017, **63**, 19–25.
24 M. Fischer and J. Georges, *Chem. Phys. Lett.*, 1996, **260**, 115–118.
25 D. Magde, R. Wong and P. G. Seybold, *Photochem. Photobiol.*, 2002, **75**, 327–334.
26 J. Shen and R. D. Snook, *Chem. Phys. Lett.*, 1989, **155**, 583–586.
27 J. Olmsted III, *J. Phys. Chem.*, 1979, **83**, 2581–2584.
28 A. M. Brouwer, *Pure Appl. Chem.*, 2011, **83**, 2213–2228.
29 M. Warzecha, J. Calvo-Castro, A. R. Kennedy, A. N. Macpherson, K. Shankland, N. Shankland, A. J. McLean and C. J. McHugh, *Chem. Commun.*, 2015, **51**, 1143–1146.
30 O. Wallquist and R. Lenz, *Macromol. Symp.*, 2002, **187**, 617–629.
31 M. Grzybowski and D. T. Gryko, *Adv. Opt. Mater.*, 2015, **3**, 280–320.
32 W. Li, L. Wang, H. Tang and D. Cao, *Dyes Pigments*, 2019, **162**, 934–950.
33 Q. Liu, S. E. Bottle and P. Sonar, *Adv. Mater.*, 2020, **32**, 1903882.
34 W. W. Bao, R. Li, Z. C. Dai, J. Tang, X. Shi, J. T. Geng, Z. F. Deng and J. Hua, *Front. Chem.*, 2020, **8**, 679.
35 Y. Li, P. Sonar, L. Murphy and W. Hong, *Energy Environ. Sci.*, 2013, **6**, 1684–1710.
36 D. Chandran and K.-S. Lee, *Macromol. Res.*, 2013, **21**, 272–283.
37 S. M. Lima, J. A. Sampaio, T. Catunda, A. C. Bento, L. C. M. Miranda and M. L. Baesso, *J. Non-Cryst. Solids*, 2000, **273**, 215–227.
38 J. Shen, R. D. Lowe and R. D. Snook, *Chem. Phys.*, 1992, **165**, 385–396.
39 M. Baesso, A. Bento, A. Andrade, J. Sampaio, E. Pecoraro, L. Nunes and T. Catunda, *Phys. Rev. B - Condens. Matter Mater. Phys.*, 1998, **57**, 10545–10549.
40 J. Calvo-Castro and C. J. McHugh, *J. Mater. Chem. C*, 2017, **5**, 3993–3998.
41 J. Calvo-Castro, C. J. McHugh and A. J. McLean, *Dyes Pigments*, 2, **113**, 609–617.
42 H. Ishida, S. Tobita, Y. Hasegawa, R. Katoh and K. Nozaki, *Coord. Chem. Rev.*, 2010, **254**, 2449–2458.
43 S. E. Bialkowski, *Photothermal Spectroscopy Methods for Chemical Analysis*, Wiley, New York, 1996, vol. 134.
44 S. L. Vadas and D. C. Fritts, *J. Geophys. Res. Atmospheres*, 2005, **110**, 1–16.
45 C. Jacinto, S. M. Lima and T. Catunda, 2005, vol. 125, pp. 225–227.
46 J. V. Caspar and T. J. Meyer, *J. Phys. Chem.*, 1983, **87**, 952–957.
47 J. V. Caspar, B. P. Sullivan, E. M. Kober and T. J. Meyer, *Chem. Phys. Lett.*, 1982, **91**, 91–95.
48 R. Englman and J. Jortner, *Mol. Phys.*, 1970, **18**, 145-.
49 M. Bixon, J. Jortner, J. Cortes, H. Heitele and M. E. Michelbeyerle, *J. Phys. Chem.*, 1994, **98**, 7289–7299.